Catalysis Science & Technology

Accepted Manuscript

ROYAL SOCIETY OF CHEMISTRY

www.rsc.org/catalysis

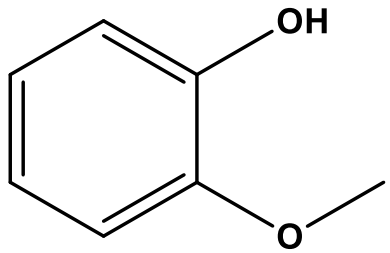

guaiacol

Biomass derived
lignin model compound

Hydrodeoxygenation

Single layered
MoS_2/C catalyst

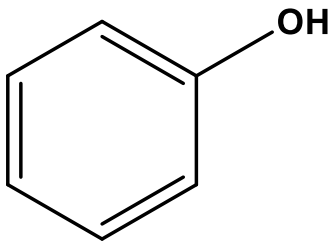

phenol

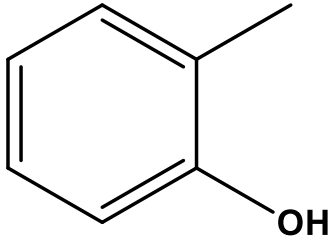

cresol

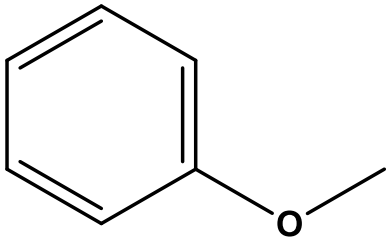

anisole

Aromatic chemicals

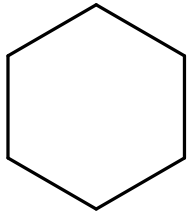

cyclohexane

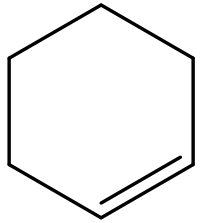

cyclohexene

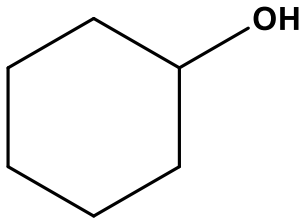

cyclohexanol

Fuels

- Single layered MoS_2 supported on activated carbon prepared by microemulsion technique
- Good catalyst stability even after 4 uses

Journal Name

ARTICLE

Guaiacol hydrodeoxygenation reaction catalyzed by highly dispersed, single layered MoS_2/C

Received 00th January 20xx,
Accepted 00th January 20xx

DOI: 10.1039/x0xx00000x

www.rsc.org/

Swathi Mukundan,[a] Muxina Konarova,[a] Luqman Atanda,[a] Qing Ma,[a] and Jorge Beltramini*[a]

A highly disordered MoS_2, dispersed on carbon support was prepared by microemulsion technique and its application as a catalyst for hydrodeoxygenation of guaiacol, a typical model compound of lignin, was investigated. The deoxygenation reaction was the predominant route producing phenol as a major product. It is also demonstrated that the single layered MoS_2/C catalyst showed superior activity and better deoxygenation and hydrogenation properties than the stacked MoS_2/C. Reusability test showed good catalyst stability after 4 catalytic cycles were performed. Catalyst surface morphological changes, sulphur loss and its effect on conversion of guaiacol and selectivity of products were studied using multiple analytical methods such as TEM, XPS, CHNS, N_2 adsorption and Raman. The performance of the MoS_2 based catalyst during the guaiacol HDO reactions demonstrated its potential for upgrading of lignin.

1. Introduction

Lignin, a component of biomass is an abundant renewable source that is freely available everywhere. It has a unique structure and chemical properties that makes it a potential source of a wide range of bulk and fine chemicals particularly aromatic compounds as well as transportation fuel precursors and additives.[1] Lignin deoxygenation reaction is a promising route to valuable chemical conversions.[2] This strategy can be achieved by adapting the traditional hydrotreating reaction of hydrocarbons employed in the petroleum refineries. The process involves the removal of heteroatoms such as oxygen, nitrogen and sulphur atoms in the presence of hydrogen by hydrodeoxygenation, hydrodenitrogenation and hydrodesulphurization reactions which are usually accompanied by hydrogenation of aromatic compounds to produce fuels.[3] An effective hydrotreating catalyst must have the potential to achieve a high conversion at mild reaction conditions in order to reduce coke formation, while the catalyst should selectively deoxygenate without excessive hydrogen consumption during hydrogenation.[4] A number of reviews have been dedicated for lignin depolymerization studies.[5-8] Lignin pyrolysis usually takes place at a temperature range of 280-500 °C, wherein substituted phenols were obtained resulting from cleavage of ether and C-C linkages.[9] Lignin-derived phenolic compounds are of great interest in the chemical industries as they can be used to manufacture synthetic bioplastics such as phenolic resins, epoxides, adhesives and polyolefins.[10] Complete deoxygenation and hydrogenation of lignin gives liquid hydrocarbon fuels such as cyclohexane. Due to the complex structure of lignin, low molecular weight model compounds such as guaiacol has been successfully used for easy interpretation of the kinetics, reaction pathway and stability of the products during lignin depolymerization.[11, 12]

Supported noble metal catalysts have shown potential applications for HDO reaction studies. It was found that Rh/ZrO_2 serves as a superior catalyst for the complete hydrogenation of guaiacol.[13] Elliott et al.[4] tested the hydroprocessing capacity of Ru and Pd catalyst for biomass model compounds and they established that hydrogenation occurs at 100 °C, whereas 300 °C is the optimum temperature for deoxygenation. Wildschut et al.[14] reported that Ru/C is a promising catalyst for deoxygenation and hydrogenation. Similarly, it was found that ReS_2/C was capable of C-O bond cleavage, producing phenol from guaiacol.[15] Despite the attractiveness of utilizing noble metal as HDO catalysts, the high cost of precious metal and relatively high H_2 pressure required for the catalytic lignin depolymerization process makes it unfavourable for commercialization.

On the contrary, Ni or Co promoted MoS_2 supported on alumina has been used as a hydrotreating catalyst where MoS_2 edges acts as the primary catalytic active sites.[16, 17] The promotional role of Co or Ni is to lower the binding energy of sulphur at the edges of MoS_2, thereby increasing vacant sites.[18] A number of studies have been reported on the activity of unmodified and modified (using alkaline and precious metals) sulfided CoMo and NiMo catalysts, for the hydrodeoxygenation, dehydrogenation and hydrogenolysis of model molecules representative of bio-oils.[19-21] Sulphided $CoMo/Al_2O_3$ promotes deoxygenation of guaiacol giving phenol and catechol as major products.[22] However Al_2O_3 is not a good

[a] Nanomaterials center- AIBN and school of chemical engineering, The University of Queensland, Brisbane, QLD-4072, Australia.

† Electronic Supplementary Information (ESI) available: The details containing figures of TPR, XPS, EDX analyses, catalyst activity and Table of Raman frequencies and XPS binding energies. See DOI: 10.1039/x0xx00000x

support because it tends to deactivate very fast when water is formed in the hydrodeoxygenation reaction.[23] Laurent et al.[24] also observed the deactivation of sulphided $NiMo/Al_2O_3$ led to decline in activity during HDO of guaiacol. The authors established that alumina irreversibly undergoes partial crystallization to form bohemite. Also the presence of weak Lewis acid sites on the alumina support is responsible for increase in coke formation.[24] These findings paved the way to seek alternative supports for transition metal sulphides. Carbon can offer many advantages as a support because of its good resistant to acid and base media, amphoteric nature that facilitates metal adsorption and catalyst dispersion, low cost and high thermal stability. [25-27] It also has a unique advantage of ease of active metal recovery from catalysts by simply oxidizing carbon into its oxides.[28, 29] Most importantly, carbon has less affinity to produce coke when compared to the acidic supports for HDO reactions.[30-33]

It is established that acidity of support has a significant influence on catalyst selectivity.[34-36] Lee et al.[37] reported that Pt, Pd, Ru and Rh when supported on carbon black treated with nitric acid selectively enhance production of 2-methyl cyclohexanol. However, when the same metals were supported on Al_2O_3 and SiO_2-Al_2O_3, deoxygenation reaction pathway was promoted due to the availability of more acid sites, giving more cyclohexane.[37] These catalysts can be considered as bifunctionals, consisting of acid and metal sites which are responsible for deoxygenation and hydrogenation respectively. Nimmanwudipong et al.[38] also examined the catalytic conversion of guaiacol with Pt/Al_2O_3 and concluded that acidic support promotes alkyl group migration resulting in alkylated product. Ru/MgO catalyst was shown to be capable of selectively producing cyclohexanol and methanol from guaiacol. However, in the absence of MgO, the yield of cyclohexanol is lower and more methane is produced. The basic site of MgO support promotes dealkylation and a decrease in gas formation.[39] The support acidity effect was also explored by Bui et al.[40] where the activity of MoS_2 supported on different materials such as Al_2O_3, TiO_2 and ZrO_2 was tested for the HDO of guaiacol in a continuous fixed bed reactor. They found catechol as the major product along with methylated compounds with MoS_2/Al_2O_3. However when using TiO_2 and ZrO_2 as catalyst support which are less acidic in nature, phenol and catechol were found to be the most product along with cyclohexene.[40] The activity of CoMo supported on two different supports such as Al_2O_3 and carbon was compared and found that the CoMo/C produces higher phenol/catechol ratio and less coke formation but lesser conversion when compared with that of $CoMo/Al_2O_3$.[41] The weak metal-support interaction effect found in CoMoS/C catalyst is responsible for its higher catalytic selectivity compared with the metal oxide alumina supported catalyst.[42] Carbon supported catalysts favours demethoxylation, thus producing phenol directly from guaiacol.[40] Mainly, the coke formation was negligible over carbon supported CoMoS catalyst for the HDO reaction of guaiacol.[43] MoS_2 supported on different carbon supports has been tested for HDO of guaiacol and it was found that the surface functionality of the support has great effect on the selectivity.[44]

The morphology of MoS_2 also plays an important role in the catalyst activity and selectivity.[45] Daage et al.[46] proposed a rim-edge model for MoS_2 particles and concluded that the top and bottom edge planes are responsible for hydrogenation whereas all the edge planes are responsible for hydrogenolysis. Hensen et al.[47] also reported that hydrogenation takes place predominantly with highly stacked MoS_2 particles. Yang et al.[48] examined the effect of morphology of MoS_2 for the HDO of phenol and concluded that low stacked MoS_2 favours hydrogenolysis. The Mo active phase accessibility and dispersion over the support also influences the activity of the catalyst.[49] This conclusion was also abided by Sepulveda et al.[50] who also found that surface chemistry of the carbon support has impact on active phase dispersion.

As such MoS_2 catalysts for hydrotreating purpose are usually synthesised by impregnation of molybdenum precursor over the support, followed by external sulphidation by introducing H_2S. In such cases, the hydrogen sulphide partial pressure deeply affects the catalyst activity.[51] This method of synthesis usually results in ordered crystalline multi-layered slabs of MoS_2 over the support. However the defective amorphous MoS_2 results in more unsaturated S atoms at the edges thereby increasing the active sites available for reaction.[52, 53] On the other hand, microemulsion (ME) is a well-known technique for synthesizing nanosized metal catalysts. For example, Ru/γ-Al_2O_3 synthesized by ME was reported to produce more hydrogen from bagasse when compared to that prepared by impregnation technique.[54] $NiMoS_2$/laponite synthesised by ME has also been demonstrated to have a higher hydrogenating activity during syngas to ethanol reaction.[55]

In this paper, we report a microemulsion (ME) synthesis of a highly dispersed and disordered nanosized MoS_2 supported on activated carbon. We also demonstrated its application as a catalyst for guaiacol HDO reaction, targeting mainly phenol and cyclohexane production.

2. Materials and methods

2.1. Materials

Brij 30, ammonium molybdate tetrahydrate ($(NH_4)_6Mo_7O_{24}.4H_2O$), ammonium sulphide solution (20%), dodecane, guaiacol, cyclohexane, cyclohexene, anisole, veratrole, cresol, activated carbon (C) as support (activated charcoal, norit SX ultra, from peat) were purchased from Sigma-Aldrich.

2.2. Catalyst synthesis

Carbon supported MoS_2 catalysts were prepared by microemulsion (ME) technique. For the synthesis, non-ionic brij-30 surfactant was added to cyclohexane (1:20 wt. %) under stirring until complete dissolution. The resulting solution is referred to as an oil phase. Thereafter, 5 mL of ammonium

sulphide solution was added to the oil phase and stirred for 1 h. This was followed by dropwise addition of 2 mL aqueous solution of ammonium molybdate tetrahydrate to the mixture, which then turns black. The concentration of molybdenum was calculated as 12 wt. %. Activated carbon was used as a support and this was added to the above mixture and stirred for 1 h, resulting in the deposition of the MoS_2 over the support. The cyclohexane was then slowly evaporated at room temperature and the final product was thermally treated at 550 ºC for 4 h under N_2 to get the carbon supported MoS_2 nanoparticles, which was labelled as MoS_2/C. MoO_x/C was prepared following the same procedure as MoS_2 but without the addition of ammonium sulphide.

2.3. Catalyst characterisation

The surface area and pore volume were measured by Nitrogen adsorption-desorption isotherms and obtained at -196 ºC by using a Micrometrics Tristar II 3020 system. The catalysts were degassed at 200 °C overnight on a vacuum line. The catalyst morphology was characterised by Transmission Electron Microscopy (TEM) using a JOEL 2100 microscope operated at 200Kv, fitted with a JEOL thin-window energy dispersive X-ray (EDS) detector. The bulk composition of the catalyst was determined by Inductively Coupled Plasma (ICP) analysis in a Varian Vista Pro ICPOES instrument, after digesting the catalyst using a milestone Ethos 1 microwave digester. The amount of sulphur on the catalysts after each reaction cycle during reusability study was analysed by CHON-S analyser (FLASH EA 1112 series, Thermo Electron Corporation). X-ray diffraction (XRD) patterns were recorded on Rigaku Miniflex with monochromatic Co Kα radiation at 30kv and 15 mA with a step size of 0.1 °. A Kratos Axis ULTRA X-ray photoelectron spectrometer associated with 165 mm hemispherical electron energy analyser and Al Kα X-rays (1486.6 eV) incident radiation was also used to investigate catalyst surface composition before and after reaction. Casa XPS version 2.3.14 and a Shirley baseline was used for curve fitting. Peak positions were calibrated by taking C *1s* line in carbon spectra at 284.8 eV as a reference. Sample analysis by Raman spectroscopy was performed using Renishaw inVia Raman Microscope under ambient conditions. The pump radiation was supplied by Argon green laser operating at a wavelength of 514 nm and 0.1 mW laser power. The Raman emission was collected by 50x objective in a backscattering geometry. Temperature programming reduction (TPR) was performed using the setup described elsewhere.[56]

2.4. Catalytic tests

The catalytic hydrodeoxygenation (HDO) reaction of guaiacol was performed in 300 mL stainless steel stirred reactor by Parr instrument. Prior to reaction, the catalysts were pretreated under hydrogen flow in a continuous flow reactor at 450 ºC for 3 h (flow rate: 20 mL/min) under hydrogen flow to remove sulphate groups. The pretreated catalyst is allowed to cool down under nitrogen flow before being transferred into the reactor. In a typical reaction, the reactor was loaded with appropriate amount of guaiacol (reactant), dodecane (solvent) and the catalyst (catalyst:guaiacol mass ratio = 1:20, 1:10, 1:6.7, 1:5). The reactor was purged and flushed with argon to evacuate air and pressurised with H_2 to 50 bar (H_2:guaiacol initial mole ratio- 11:1). The temperature is then heated to 300 °C. The reaction starts when the set temperature is reached, and is allowed to run for 5 h. During the course of the reaction, the pressure and temperature were monitored. Liquid and gas sampling were done at an hourly interval. At the end of the reaction, the reactor was stopped and cooled, and the catalyst was recovered by filtration from the reaction product. The recovered catalyst was washed with ethanol, dried at 50 °C overnight and then reused for the stability/reusability study. There was some unavoidable loss of catalyst during filtration. This loss was compensated for by adding fresh catalyst to the recovered catalyst while carrying out the reusability study. The reusability test was conducted with the same catalyst for four reaction cycles under similar reactions conditions. The fresh catalyst is represented as MoS_2/C- fresh and the catalyst after each cycle is represented as cycle 1, cycle 2, cycle 3 and cycle 4 respectively.

2.5. Product analysis

The products were analysed using a gas chromatography unit from (Shimadzu GC-17A) equipped with flame ionisation detector (FID) and CP-Sil 5 CB capillary column (30m×0.25mm×0.39m). The standards for guaiacol and other products were prepared in ethyl acetate.

Conversion (%C) of guaiacol, product selectivity (%S) and yield (%Y) were calculated in mol % as follows:

$$\%C = \left(1 - \frac{\text{Number of moles of guaiacol in product}}{\text{Initial moles of guaiacol in feed}}\right) * 100$$

$$\%Y = \left(\frac{\text{Number of moles of the product}}{\text{Initial moles of guaiacol in feed}}\right) * 100$$

$$\%S = \left(\frac{\text{Number of moles of the product}}{\text{Number of converted moles of guaiacol}}\right) * 100$$

3. Results and discussion

3.1. Catalyst characterization

The N_2 adsorption-desorption isotherm and pore size distribution plots of MoS_2/C, activated carbon and unsupported MoS_2 are shown in Fig. 1. The results of surface area, pore size and pore volume of the samples are also presented in Table 1.

The BET surface area of activated carbon was found to be 1063 m^2/g and 66 % of this value corresponds to micropore area. Unsupported MoS_2 has a surface area of 167.1 m^2/g and a pore size of 4 nm. Meanwhile, the surface area of MoS_2 reduced to 126 m^2/g when supported on activated carbon (MoS_2/C). This behaviour can be ascribed to the blockage of micropore of carbon by MoS_2 species during synthesis.[57]

Table 1 BET surface area, pore volume, pore size of activated carbon, unsupported MoS_2 and MoS_2/C catalysts

Samples	BET Surface area (m^2g^{-1})		Pore Volume (cm^3g^{-1})		Pore Size (nm) [b]
	Micro[a]	Total	Micro	Total	
Activated carbon	705	1063	0.36	0.98	3.95
Unsupported MoS_2	35	167	0.02	0.21	4.0
MoS_2/C	17.5	126	0.01	0.27	3.8

[a]Calculated from BET t-Plot micropore area, [b]pore size calculated by BJH method from desorption isotherm.

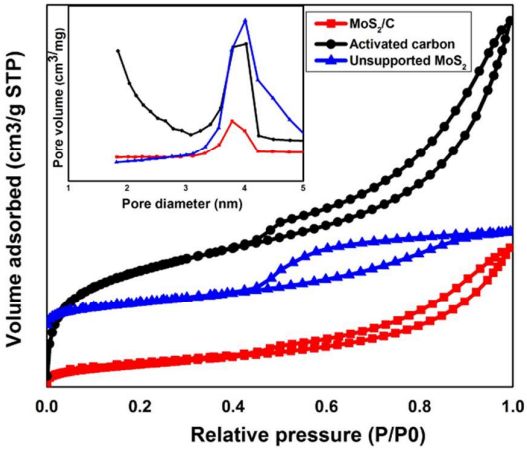

Fig. 1 Nitrogen adsorption isotherm and pore size distribution curves of unsupported MoS_2, MoS_2/C- fresh and activated carbon

It has been reported that MoS_2 exists as a stacked layered material with up to seven layers.[58] By using the microemulsion preparation route, we were able to produce highly dispersed single layered MoS_2 on the activated carbon support. The absence of stacked layers was also confirmed by the XRD result, in which their corresponding peak at $2\theta = 16.7°$ was not detected (Fig. 2). The TEM image of unsupported MoS_2 reveals the presence of layered MoS_2 particles, suggesting the occurrence of a maximum of 2 layered structure (Fig. 3a). When MoS_2 is supported on activated carbon, a uniformly dispersed MoS_2 species of single layer was formed having an average slab length of 4 nm (Fig. 3b).

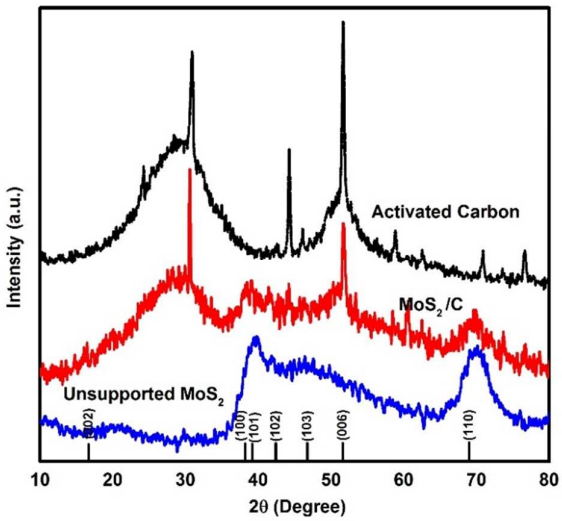

Fig. 2 X-ray diffraction pattern of MoS_2/C, unsupported MoS_2 and activated carbon

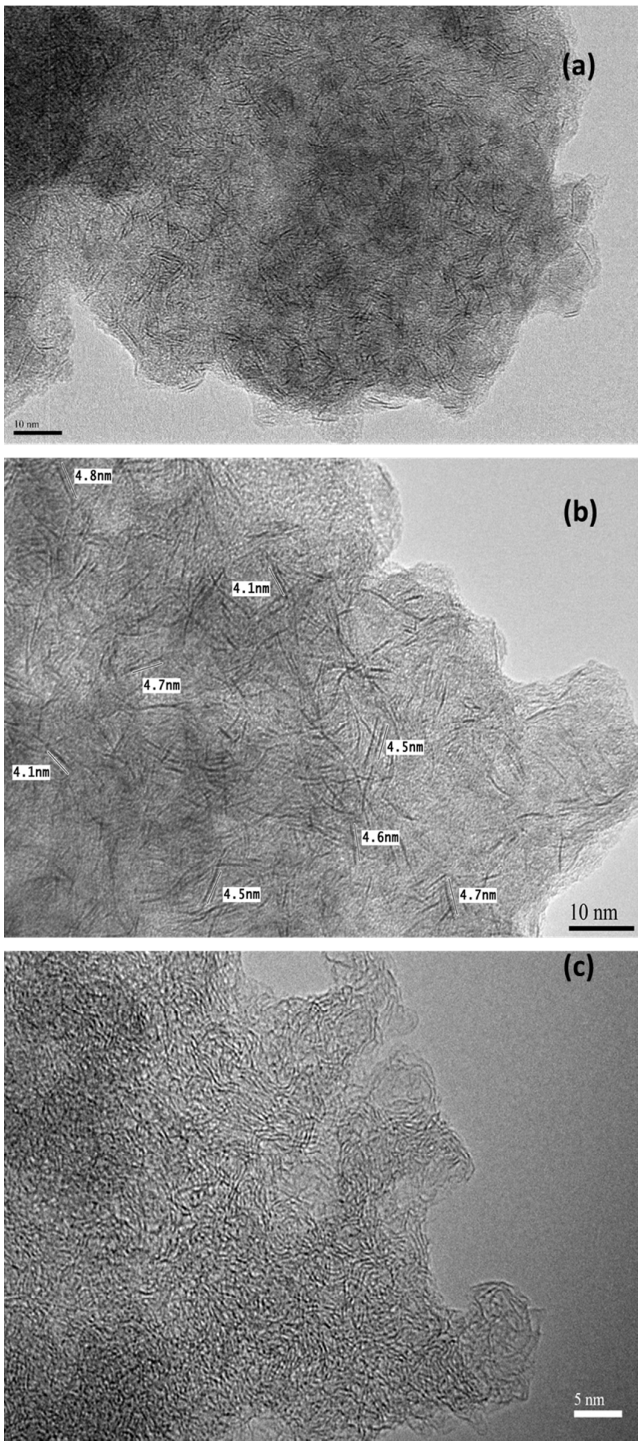

Fig. 3 HR-TEM images of a) UnsupportedMoS_2 b) MoS_2/C c) Activated carbon

3.2. Hydrodeoxygenation (HDO) of guaiacol over MoS_2/C catalyst

Firstly, the guaiacol HDO reaction was conducted at 300 °C in the absence of a catalyst to check the influence of thermal conversion of guaiacol. It is noteworthy to mention that it took 13 min to ramp from room temperature to the reaction temperature (300 ˚C) and the pressure increased from 50 bar to 60 bar. This increase in pressure could be due to the rise in temperature. From this test result, only 10 % guaiacol conversion was achieved producing mainly catechol and a small trace of phenol. Similar result was also reported by Ceylan et al.[36]

Prior to the catalytic test, MoS_2/C (catalyst: guaiacol mass ratio= 1:10) was pre-treated under pure H_2 flow at 450 °C for 3 h. This pre-treatment eliminates SO_2 which was formed as a result of the presence of atmospheric oxygen during ME synthesis. The elimination of SO_2 after pretreatment was confirmed by TPR and XPS analyses (Fig. 1, 2 in ESI†). The catalytic performance of the pretreated catalyst was examined for the hydrodeoxygenation of guaiacol, and the result is illustrated in Fig.4. During the temperature ramping period from room temperature to reaction temperature, the pressure rose from 50 bar to 85 bar. We can infer that the 35 bar rise in pressure during reaction is a contribution of both temperature rise and gaseous products released due to guaiacol conversion.The time the final temperature (300 ˚C) was reached, reaction was considered to be started. At this stage, 2.5 % guaiacol conversion has already been attained, producing liquid products consisting of phenol, catechol and cresol with selectivities of 35 %, 17 % and 1.8 %, respectively.

The products formed during the guaiacol HDO reaction catalysed by MoS_2/C can be grouped into four categories:

i. *Deoxygenated products* - phenol, anisole and benzene.
ii. *Hydrogenated products* - cyclohexane, cyclohexene, cyclohexanol.
iii. *Methylated products*- veratrole, cresol.
iv. *Gaseous products*- methane, CO, CO_2.

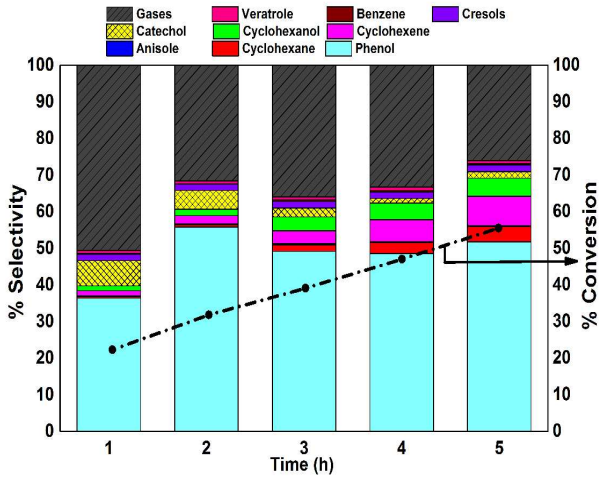

Fig. 4 Conversion and product selectivity of guaiacol HDO reaction catalyzed by MoS_2/C at reaction conditions of 300˚C and 50 bar for 5 h.

Table 2 Selectivity of main liquid products of guaiacol HDO reaction catalyzed by MoS_2/C at reaction conditions of 300°C and 50 bar at 5 h.

Product	Selectivity (%)
Phenol	52
Cyclohexane	4.2
Cyclohexene	8
Cyclohexanol	5
Anisole	0.3
Cresols	1.2
Benzene	0.4
Catechol	1.8
Veratrole	0.8
Methanol	0.04

A complete major liquid product distribution is given in Table 2. According to previous reports, guaiacol can undergo two pathways to produce phenol: 1) Demethylation of guaiacol to produce catechol giving CH_4 or CH_3^+ as the sub product. Then, successive deoxygenation of catechol to give phenol and water[59] or 2) Direct demethoxylation to produce phenol with methanol as a side product.[51, 60, 61]

From our results, the rupture of O-CH_3 bond of guaiacol molecule takes place initially to produce catechol. This is justified by the observed high selectivity towards catechol and methane.[19] Hurff and Klein[22] suggested a similar pathway for guaiacol HDO by CoMo/γ-Al_2O_3. Phenol is then produced from catechol via deoxygenation i.e. elimination of hydroxyl group. From Fig. 4, we can see that the selectivity towards catechol goes through a maximum in the first one hour and then decline, further confirming deoxygenation of catechol to phenol. Meanwhile, another plausible reaction pathway for phenol production is the direct demethoxylation of guaiacol to phenol and methanol. However, in our case, the amount of methanol formed as a by-product is very less. This might be due to the fast decomposition of the methanol to methane during the reaction. So, we can say that demethylation and demethoxylation of guaiacol takes place simultaneously. At this stage, it is not categorical which reaction pathway of phenol formation predominates, and this is a subject of further investigation.

Phenol/catechol ratio is largely influenced by acidity of the catalyst support used. Sepulveda et al.[62] reported that ReS_2/Al_2O_3 produce more catechol and methylated products when compared to ReS_2/SiO_2. Bui et al.[40] also observed a similar result when comparing $CoMoS/ZrO_2$ and $CoMoS/Al_2O_3$. From these results, we can conclude that strong acidic sites favour demethylation to catechol whereas weaker acidic sites favour demethoxylation to phenol.

When we examined the effect of MoS_2 morphology on the phenol/catechol ratio, we found that single layered MoS_2/C produces less catechol in comparison to a multi-layered, stacked MoS_2/C. Ruiz et al.[44] observed that for a multi-layered stacked MoS_2/C, catechol and phenol (phenol/catechol = 0.31) were the main products, with less selectivity towards hydrogenated products. In our case, a single layered MoS_2/C obtained by microemulsion synthesis gave a phenol/catechol ratio of 5.3 in the first 1 h of the reaction which later increased by approximately 10 folds to a ratio of 50 at the end of the reaction, suggesting that catechol was initially formed and then deoxygenates as the reaction proceeds. Hence, we can infer from this result that single layered MoS_2 particles enhance deoxygenation and hydrogenation reactions faster than multi layered MoS_2 in producing phenol.

Furthermore, we observed that phenol undergoes methylation to cresol. The CH_3^+ which was formed as a side product during the catechol formation, reacts with guaiacol and phenol, producing veratrole and cresols respectively as a result of methylation.[15] Initial cresol selectivity was 1.8 % without any further change throughout the reaction whereas veratrole selectivity increased gradually with reaction time giving a maximum selectivity of 0.8 %. This result indicates mild alkylation of guaiacol and phenol which may be assumed to be insignificant.

Phenol undergoes mainly two reaction pathways:

1) Deoxygenation by breaking C-O bond, giving benzene.
2) Hydrogenation of the aromatic ring, producing cyclohexanol, followed by the elimination of OH groups.[63]

We noticed that hydrogenation of phenol begins after the first one hour of reaction, forming cyclohexanol via cyclohexanone as an intermediate. Zhao et al.[64] also reported a similar hydrogenation pathway of phenol to cyclohexanol on Pd/C catalyst. Hydrogenolysis of phenol to benzene was minimal. No cyclohexane was observed, suggesting there was no hydrogenolysis of cyclohexanol taking place. No heavier methylated products was identified. The reaction pathway summarizing the observable products of HDO of guaiacol is shown in scheme 1, similar to the scheme proposed by Bui et al.[40] The authors proposed that demethoxylation, demethylation and methylation of guaiacol takes place at the onset of the reaction, followed by hydrogenation of the intermediate products. However, we did not detect the formation of heavy products such as methyl catechol.[65]

Scheme. 1 HDO reaction pathway of guaiacol over MoS_2/C catalyst

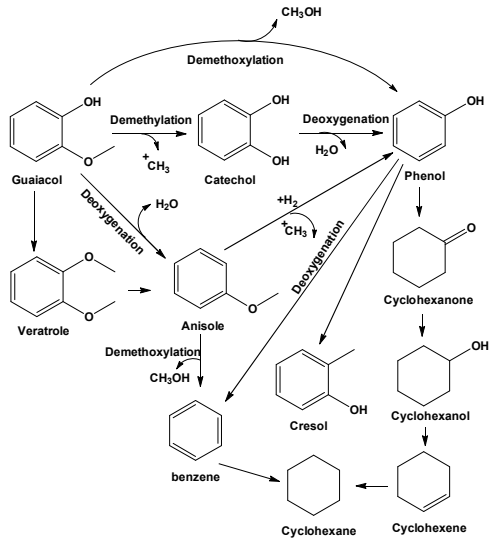

3.3. Effect of catalyst loading on guaiacol HDO reaction

The effect of MoS_2/C catalyst loading during the HDO reaction was tested under the same reaction conditions described above and the results at fifth hour reaction time are presented in Fig 5a and 5b. From the figures, we observed that at 5 wt. % catalyst loading (catalyst:guaiacol = 1:20), guaiacol conversion was 39 % and the main products are phenol and methane. When the catalyst loading was increased to 10 wt. % (catalyst:guaiacol = 1:10), conversion increased to 55 % concurrently with increased selectivity towards phenol and hydrogenated products such as cyclohexane, cyclohexene and cyclohexanol. The generated methane gas alkylates with phenol and guaiacol to form veratrole and cresol, respectively. Further increment in catalyst loading to 15 and 20 wt. % (catalyst: guaiacol = 1:6.7 and 1:5), resulted in increased conversion to 78 % and 86 %, respectively. However, selectivity of phenol and cyclohexane (desired products) were similar to that of 10 wt. % catalyst loading. Based on the fact that selectivity of desired products remain unchanged after 10 wt. % catalyst loading, we concluded that optimum catalyst to guaiacol ratio is 1:10 (10 wt. % catalyst loading) and hence, further catalytic studies were conducted using this ratio.

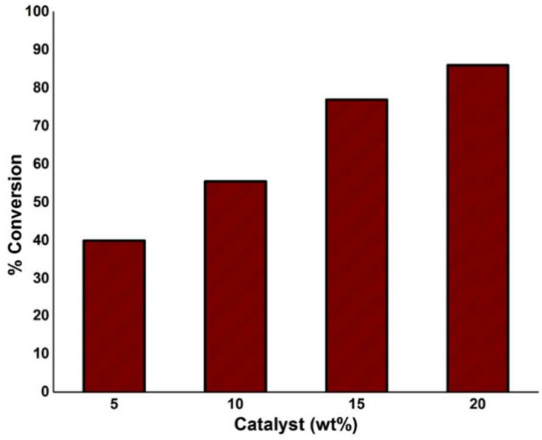

Fig. 5a Effect of catalyst wt. % (loading) on the conversion of guaiacol catalyzed by MoS_2/C catalyst

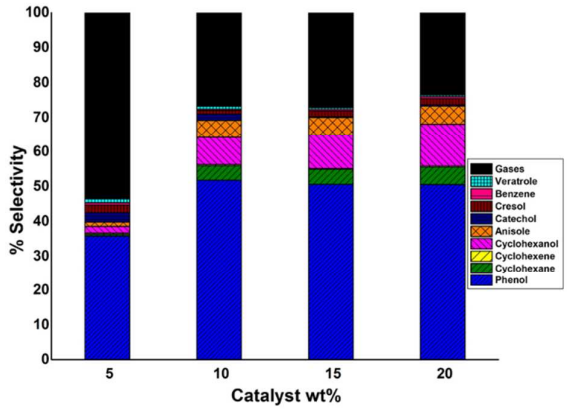

Fig. 5b Effect of catalyst wt. % (loading) on product selectivity in the HDO of guaiacol catalyzed by MoS_2/C

3.4. Catalyst reusability study

The MoS_2/C catalyst was subjected to reusability test by recycling the same catalyst for four consecutive cycles for guaiacol HDO reaction. At the end of each cycle, the catalyst was recovered from the feed by filtration and dried overnight at 50 °C. There was about 2-4 % catalyst loss during the filtration. This catalyst loss was compensated for by adding fresh catalyst. Result of the reusability test is shown in Fig. 6. From the data, we observed that guaiacol conversion drops consecutively with each cycle from 56 % after cycle-1 to 39 % after cycle-4. However, the selectivity of the products altogether remain unchanged (Fig. 3 in ESI†). The selectivity of phenol was similar for all the cycles whereas the selectivity of hydrogenated products (cyclohexane, cyclohexene and cyclohexanol) decreased after successive cycles. Conversely, selectivity of methylated products (veratrole and cresols) increased after successive cycles. Nevertheless, the drop in the conversion of guaiacol has great impact on the products yield. Yield is directly proportional to the conversion, therefore when the conversion decreased, the products yield also decreased. From Fig. 6, we noticed that the yield of phenol and hydrogenated products declined while the yield of cresol and veratrole increased after each cycle. Also, there was decline in the hydrogenation and hydrogenolysis of guaiacol. This indicates that the active sites responsible for these reactions are covered by coke deposits or heavy intermediate coke precursors.

The deactivation of the noble metal catalyst supported on carbon during the HDO of guaiacol was studied by Danni Gao et. al.[66] The authors concluded that the main reason for catalyst deactivation is because of metal sintering, which is as a result of high reaction temperature as well as coke deposits formed by polyaromatics compounds. Reaction conditions such as temperature, hydrogen pressure and contact time can influence the extent of coke formation.[23] However, in the case of sulphided hydrotreating catalyst, replacement of S by O species in the catalyst may also influence catalyst deactivation.

Sulphur loss can be compensated for by introducing a sulphur source in the reaction medium such as CS_2, which helps to sustain the sulfided state of the catalyst.[44] Alternatively, the used catalyst can be sulphided before using for the next cycle.[67]

To find a possible explanation for the decrease in conversion, change in product selectivity and yield, more comparative studies were carried out on fresh and spent catalysts.

The spent catalyst was characterized to examine its morphology and elemental composition. TEM images of the spent MoS_2/C catalyst show the presence of multi-layered stacked MoS_2 species supported on carbon (Fig. 7 (a) and (b)). However, the MoS_2 particles remained dispersed over the carbon forming up to 3 layers in the bulk part of the material (Fig. 7 (c) and (d)). EDX was also used to confirm dispersion of MoS_2 on the carbon support. The EDX result showed uniform dispersion of MoS_2 species for both the fresh and spent catalysts (Fig. 4, 5 in ESI†).

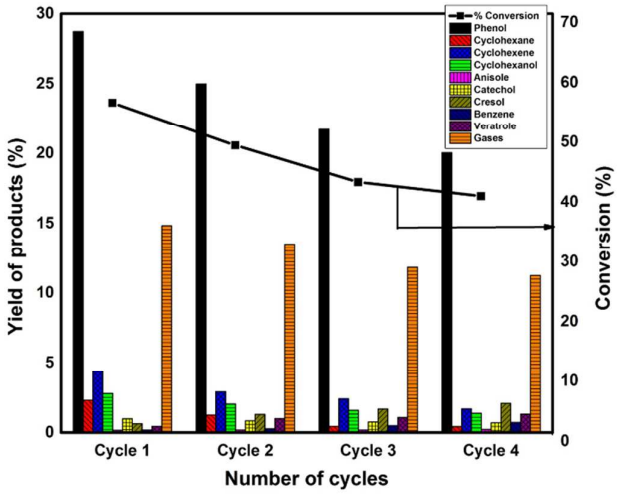

Fig. 6 Catalyst reusability study. Conversion and yield of products for HDO of guaiacol over MoS_2/C catalyst

However, with the spent catalyst, there is a significant change in slab length and number of layers of the MoS_2 nanoparticles on the support. The stacked MoS_2 appear to have fringes with an interlayer distance of approximately 0.6 nm. This observation indicates that particle growth may have occurred at some areas of the catalyst, during the successive reaction cycles, resulting in the formation of large particles, which accounts for the observed changes in conversion, product yield and selectivity as shown in Fig. 6 and Fig. 4 in ESI† respectively. It is reported that S atoms present in MoS_2 species can be mobile during the reaction, resulting in the sintering of MoS_2 particles as previously observed.[68]

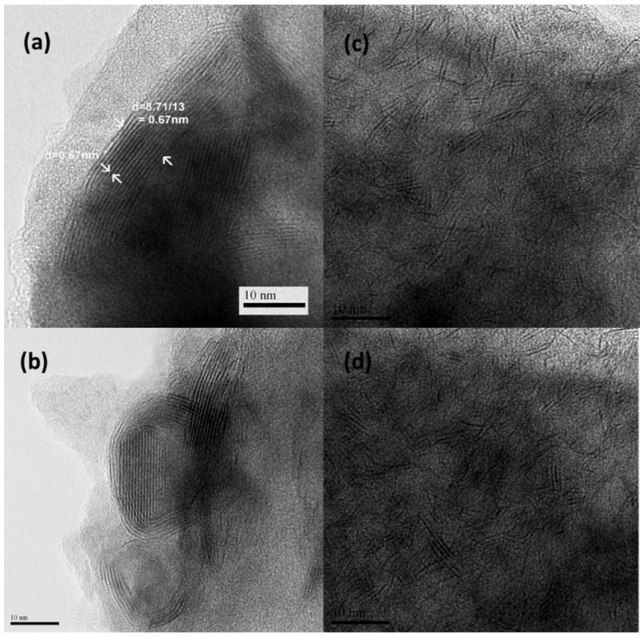

Fig. 7 HR-TEM image (a,b,c,d) of spent MoS_2/C

Table 3 BET surface area, pore size, pore volumes of fresh and used MoS_2/C catalysts

Catalyst (MoS_2/C)	BET Surface area (m^2/g)		Pore Size (nm)[b]	Pore Volume (cm^3g^{-1})	
	Micro[a]	Total		Micro	Total
Fresh	17.5	126	3.8	0.008	0.27
Cycle 1	14	111	3.7	0.007	0.25
Cycle2	12	89	3.7	0.006	0.22
Cycle3	11	85	3.65	0.005	0.21
Cycle4	11	82	3.6	0.005	0.21

[a]Calculated from BET t-Plot micropore area, [b]pore size calculated by BJH method from desorption isotherm.

BET surface area and pore volume of fresh and spent catalysts are summarized in Table 3. Comparison of BET surface area shows a significant decrease in the surface area and pore volume after successive use of the catalyst. This can be attributed to coke deposit on the catalyst surface. Leyva et al.[69] also observed that coke was deposited on the micropore surface of NiMoS/alumina catalyst during hydrocarbon hydroprocessing.

Raman spectroscopy was also used to compare the fresh and spent MoS_2/C catalysts and the result is shown in Fig. 8. We noticed that both the fresh and spent MoS_2/C catalysts showed strong signals of E^1_{2g} and A_{1g} Raman vibrations that can be ascribed to S-Mo-S layer. Raman spectroscopy is highly sensitive to number of layers and slab thickness.[70, 71] Lee et al.[72] presented the raman scattering of single and multi-layered MoS_2 samples. They reported that A_{1g} frequency shifts upwards as the number of slabs increases. Thus in our case, the A_{1g} of the fresh catalyst was 403.66cm^{-1} and it was found to be at 407.39cm^{-1} after the fourth reaction cycle. It was also reported that the intensity of Raman peaks decrease with

increase in slab number. We noticed from Fig. 8, that the Raman intensities of the fresh catalyst are strong which became weak in the spent catalyst at each reaction cycle. The summary of the E^1_{2g} and A_{1g} peak frequencies of fresh MoS_2/C and spent catalyst after each cycle are given in Table 1 in ESI†.

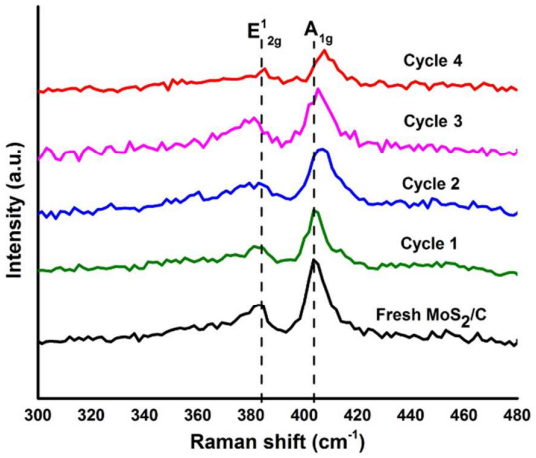

Fig. 8 Raman spectroscopy of MoS_2-fresh and spent catalyst after reaction cycles.

Table 4 Surface and bulk atomic composition (at. %) of fresh and spent MoS_2/C catalysts

Catalyst MoS_2/C	Surface atomic composition (at. %)[a]			Elemental composition (at. %)		
	Mo	S	S/Mo	Mo [b]	S [c]	S/Mo
Fresh	5.3	10.3	1.95	1.9	3.92	2.06
Cycle 1	5.6	10.5	1.89	1.9	3.88	2.04
Cycle 2	5.6	10.1	1.81	1.9	3.79	1.99
Cycle 3	6.0	10.8	1.80	1.9	3.66	1.93
Cycle 4	5.8	10.0	1.73	1.9	3.52	1.85

[a] Analysed by XPS. [b] Analysed by ICP. [c] Analysed by CHNS-O

The oxidation state and surface atomic composition of both fresh and spent MoS_2/C catalysts were analyzed by XPS. The atomic composition of the bulk material was analysed by ICP and CHNS analyses. The surface and bulk atomic composition values of fresh and spent MoS_2/C catalysts are given in Table 4. The XPS wide survey scan spectra are given in Fig. 6 in ESI†. The curve-fitted and deconvoluted spectra of high resolution scan are represented in Fig. 9. Mo 3d exhibits two oxidation states, +6 and +4, which correspond to MoO_3 and MoS_2, respectively. The XPS spectra in the Mo 3d region exhibits four characteristic peaks which can be attributed to $3d_{3/2}$ at 232.6, $3d_{5/2}$ at 229.4 for Mo (+4) and $3d_{3/2}$ at 235.8, $3d_{5/2}$ at 232.7 for Mo (+6). The small peak (Mo 3d region) at 226.8 eV represents the S (2s) bonded to Mo.[73] The S 2p displayed two $Sp_{3/2}$ doublets at 162.3 and 163.5 eV. However there is a weak broad peak at 169.8 eV which correlates with the $Sp_{3/2}$ that highlights the presence of SO_2 group. There are no significant differences in the oxidation states of Mo and S before and after reactions.

XPS binding energy values (eV) of Mo 3d and S 2p of fresh and spent MoS_2/C after each cycles is given in Table 2 in ESI†. The S to Mo ratio was found to be 1.95 for the fresh catalyst whereas the ratio decreased at the end of the reusability test, which can be ascribed to sulphur leaching. To confirm there is loss of sulphur during reaction, the CHNS analysis was also used. Surface and bulk elemental composition of Mo and S, along with the corresponding atomic ratio values are shown in Table 4.

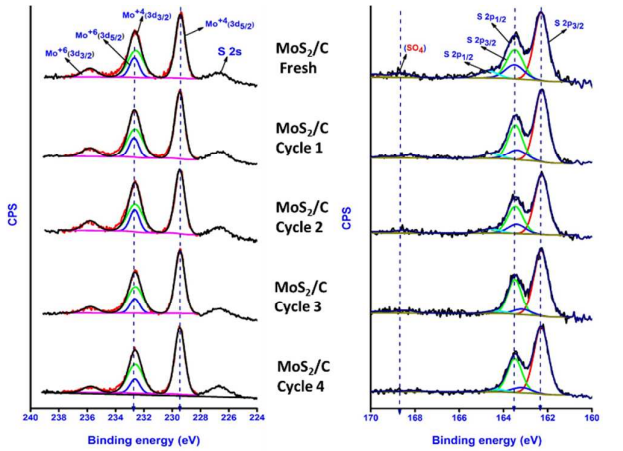

Fig. 9 Deconvoluted spectra of fresh and spent MoS_2/C catalysts (a) Mo 3d (b) S 2p regions. CPS= counts s^{-1}

From the Table, we observed that sulphur leaching occurred at all reaction cycles. ICP result shows sulphur reducing from 0.293 % (fresh) to 0.265 % (after cycle 4). However, sulphur loss may not be solely responsible for the decline in catalyst activity after consecutive cycles. It has been reported that molybdenum species become MoO_x due to sulphur loss.[55] To confirm this,

MoO_x/C was tested for the guaiacol HDO reaction and its activity was compared with MoS_2/C.

3.5. Activity comparison of MoS_2/C vs MoO_x/C for guaiacol HDO

The MoS_2/C and MoO_x/C catalysts has similar catalytic activity for guaiacol HDO reaction in the terms of conversion (52 % vs 55.5 %). However, Fig. 10 shows the difference in the product selectivity on MoO_x/C and MoS_2/C catalysts evaluated after 5 h of reaction. MoS_2/C showed high selectivity towards deoxygenated (phenol, anisole, benzene) and hydrogenated products (cyclohexane, cyclohexene, cyclohexanol) whereas MoO_x/C is more selective towards methylated products (veratrole, cresols) along with deoxygenated products. Similar result was found by Furimsky et al.[74], who reported that MoS_2/γ-Al_2O_3 produces more hydrogenated product compared to that of MoO_3/γ-Al_2O_3. The production of heavy products from methylation reaction can trigger the formation of carbon precursors on the catalyst surface.[41]

This change in selectivity for MoO_x to produce methylated products could elucidate the selectivity of producing methylated products by MoS_2/C after consecutive cycles. However, the presence of MoO_x does not affect the selectivity

towards phenol but could affect the guaiacol conversion. During HDO reaction, there is the likelihood of O atom present in the reaction feed to replace S atom of the catalyst. Thus, loss of sulphur during reaction resulted in the reduction of S/Mo ratio as observed from XPS and ICP results. After the first reaction cycle, 1.02 % of sulphur was lost. However the conversion was greatly affected, dropping from 56 % to 48 %. This loss of S results in the increase of MoO_x species in the catalyst.

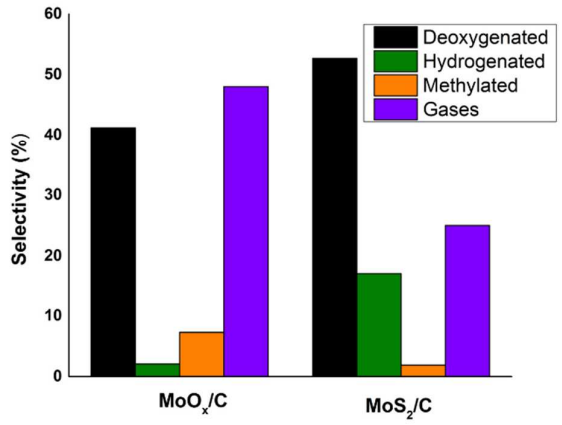

Fig. 10 Comparison of product selectivity on MoO_x/C and MoS_2/C catalysts for guaiacol HDO reaction

Conclusion

We synthesised an amorphous, single-layered MoS_2/C nanocatalyst using microemulsion technique with the purpose of elucidating its activity for guaiacol HDO reaction. The activity of the catalyst was found superior to crystalline MoS_2 catalyst synthesised by wetness impregnation method. The phenol/catechol ratio by single layered MoS_2/C is higher than stacked MoS_2/C catalyst. We also found that, MoO_x/C promotes deoxygenation along with methylation whereas MoS_2/C has better selectivity towards deoxygenation and hydrogenation. This variation in the selectivity of the oxide and sulphide catalyst could trigger changes in the activity of the catalyst. The stability of the catalytic activity of MoS_2/C for successive reaction cycles was studied and found to be affected by loss of S during reaction, metal sintering and coke deposition. The effect of promoter and its mode of introduction to the MoS_2, alongside the acidity effects is the aim of further studies and the results of which will be reported in a future publication. The catalyst synthesised proved to be promising to be used for lignin upgrading into commodity chemicals.

Acknowledgements

We thankfully acknowledge the financial support from the Nanomaterials Centre (NANOMAC), The University of Queensland. We also acknowledge the facilities and assistance provided by Center for Microscopy and Microanalysis (CMM), The University of Queensland. Finally, we acknowledge Dr. Jennifer wanders, from School of Agriculture and Food Sciences, The University of Queensland for her help with the GC-MS analysis.

Notes and references

1. G. W. Huber, S. Iborra and A. Corma, *Chemical Reviews*, 2006, **106**, 4044-4098.
2. D. C. Elliott, *Energy & Fuels*, 2007, **21**, 1792-1815.
3. H. Wang, J. Male and Y. Wang, *ACS Catalysis*, 2013, **3**, 1047-1070.
4. D. C. Elliott and T. R. Hart, *Energy & Fuels*, 2008, **23**, 631-637.
5. P. Azadi, O. R. Inderwildi, R. Farnood and D. A. King, *Renewable and Sustainable Energy Reviews*, 2013, **21**, 506-523.
6. P. de Wild, R. Van der Laan, A. Kloekhorst and E. Heeres, *Environmental Progress & Sustainable Energy*, 2009, **28**, 461-469.
7. M. Saidi, F. Samimi, D. Karimipourfard, T. Nimmanwudipong, B. C. Gates and M. R. Rahimpour, *Energy & Environmental Science*, 2014, **7**, 103-129.
8. A. L. Jongerius, P. C. A. Bruijnincx and B. M. Weckhuysen, *Green Chemistry*, 2013, **15**, 3049-3056.
9. C. Amen-Chen, H. Pakdel and C. Roy, *Bioresour Technol*, 2001, **79**, 277-299.
10. D. Stewart, *Industrial Crops and Products*, 2008, **27**, 202-207.
11. J. Zakzeski, P. C. A. Bruijnincx, A. L. Jongerius and B. M. Weckhuysen, *Chemical Reviews*, 2010, **110**, 3552-3599.
12. M. P. Pandey and C. S. Kim, *Chemical Engineering & Technology*, 2011, **34**, 29-41.
13. A. Gutierrez, R. K. Kaila, M. L. Honkela, R. Slioor and A. O. I. Krause, *Catalysis Today*, 2009, **147**, 239-246.
14. J. Wildschut, F. H. Mahfud, R. H. Venderbosch and H. J. Heeres, *Industrial & Engineering Chemistry Research*, 2009, **48**, 10324-10334.
15. C. Sepúlveda, R. García, P. Reyes, I. T. Ghampson, J. L. G. Fierro, D. Laurenti, M. Vrinat and N. Escalona, *Applied Catalysis A: General*, 2014, **475**, 427-437.
16. J. Grimblot, *Catalysis Today*, 1998, **41**, 111-128.
17. P. Afanasiev and I. Bezverkhyy, *Applied Catalysis A: General*, 2007, **322**, 129-141.
18. L. S. Byskov, B. Hammer, J. K. Nørskov, B. S. Clausen and H. Topsøe, *Catal Lett*, 1997, **47**, 177-182.
19. E. Laurent and B. Delmon, *Appl. Catal., A*, 1994, **109**, 77-96.
20. E. Furimsky, *Catalysis Reviews*, 1983, **25**, 421-458.
21. Y. Qin, L. He, J. Duan, P. Chen, H. Lou, X. Zheng and H. Hong, *ChemCatChem*, 2014, **6**, 2698-2705.
22. S. J. Hurff and M. T. Klein, *Industrial & Engineering Chemistry Fundamentals*, 1983, **22**, 426-430.
23. E. Furimsky and F. E. Massoth, *Catalysis Today*, 1999, **52**, 381-495.
24. E. Laurent and B. Delmon, *Stud. Surf. Sci. Catal.*, 1994, **88**, 459-466.
25. F. Rodríguez-reinoso, *Carbon*, 1998, **36**, 159-175.

26. in *Carbons and Carbon Supported Catalysts in Hydroprocessing*, The Royal Society of Chemistry, 2008, DOI: 10.1039/9781847558411-00040, pp. 40-47.
27. E. Lam and J. H. T. Luong, *ACS Catalysis*, 2014, **4**, 3393-3410.
28. N. Krishnankutty and M. A. Vannice, *Journal of Catalysis*, 1995, **155**, 312-326.
29. N. Krishnankutty and M. A. Vannice, *Journal of Catalysis*, 1995, **155**, 327-335.
30. A. W. Scaroni, R. G. Jenkins and P. L. Walker Jr, *Applied Catalysis*, 1985, **14**, 173-183.
31. V. H. J. de Beer, F. J. Derbyshire, C. K. Groot, R. Prins, A. W. Scaroni and J. M. Solar, *Fuel*, 1984, **63**, 1095-1100.
32. A. Centeno, E. Laurent and B. Delmon, *Journal of Catalysis*, 1995, **154**, 288-298.
33. G. W. Huber, S. Iborra and A. Corma, *Chemical reviews*, 2006, **106**, 4044-4098.
34. S. Jin, Z. Xiao, C. Li, X. Chen, L. Wang, J. Xing, W. Li and C. Liang, *Catalysis Today*, 2014, **234**, 125-132.
35. X. Zhu, L. L. Lobban, R. G. Mallinson and D. E. Resasco, *Journal of Catalysis*, 2011, **281**, 21-29.
36. R. Olcese, M. M. Bettahar, B. Malaman, J. Ghanbaja, L. Tibavizco, D. Petitjean and A. Dufour, *Applied Catalysis B: Environmental*, 2013, **129**, 528-538.
37. C. R. Lee, J. S. Yoon, Y.-W. Suh, J.-W. Choi, J.-M. Ha, D. J. Suh and Y.-K. Park, *Catalysis Communications*, 2012, **17**, 54-58.
38. T. Nimmanwudipong, R. C. Runnebaum, D. E. Block and B. C. Gates, *Catal Lett*, 2011, **141**, 779-783.
39. Y. Nakagawa, M. Ishikawa, M. Tamura and K. Tomishige, *Green Chemistry*, 2014, **16**, 2197-2203.
40. V. N. Bui, D. Laurenti, P. Delichère and C. Geantet, *Applied Catalysis B: Environmental*, 2011, **101**, 246-255.
41. E. Laurent, A. Centeno and B. Delmon, in *Studies in Surface Science and Catalysis*, eds. B. Delmon and G. F. Froment, Elsevier, 1994, vol. Volume 88, pp. 573-578.
42. J. P. R. Vissers, B. Scheffer, V. H. J. de Beer, J. A. Moulijn and R. Prins, *Journal of Catalysis*, 1987, **105**, 277-284.
43. G. de la Puente, A. Gil, J. J. Pis and P. Grange, *Langmuir*, 1999, **15**, 5800-5806.
44. P. E. Ruiz, B. G. Frederick, W. J. De Sisto, R. N. Austin, L. R. Radovic, K. Leiva, R. García, N. Escalona and M. C. Wheeler, *Catalysis Communications*, 2012, **27**, 44-48.
45. P. Ratnasamy and S. Sivasanker, *Catalysis Reviews*, 1980, **22**, 401-429.
46. M. Daage and R. R. Chianelli, *Journal of Catalysis*, 1994, **149**, 414-427.
47. E. J. M. Hensen, P. J. Kooyman, Y. Van der Meer, A. M. Van der Kraan, V. H. J. De Beer, J. A. R. Van Veen and R. A. Van Santen, *Journal of Catalysis*, 2001, **199**, 224-235.
48. Y. Q. Yang, C. T. Tye and K. J. Smith, *Catalysis Communications*, 2008, **9**, 1364-1368.
49. M. Ferrari, B. Delmon and P. Grange, *Microporous and Mesoporous Materials*, 2002, **56**, 279-290.
50. C. Sepúlveda, K. Leiva, R. García, L. R. Radovic, I. T. Ghampson, W. J. DeSisto, J. L. G. Fierro and N. Escalona, *Catalysis Today*, 2011, **172**, 232-239.
51. M. Ferrari, R. Maggi, B. Delmon and P. Grange, *Journal of Catalysis*, 2001, **198**, 47-55.
52. D. Merki and X. Hu, *Energy & Environmental Science*, 2011, **4**, 3878-3888.
53. T. F. Jaramillo, K. P. Jørgensen, J. Bonde, J. H. Nielsen, S. Horch and I. Chorkendorff, *Science*, 2007, **317**, 100-102.
54. M. Barati, M. Babatabar, A. Tavasoli, A. K. Dalai and U. Das, *Fuel Process. Technol.*, 2014, **123**, 140-148.
55. M. Konarova, F. Tang, J. Chen, G. Wang, V. Rudolph and J. Beltramini, *ChemCatChem*, 2014, **6**, 2394-2402.
56. A. Tanksale, J. N. Beltramini, J. A. Dumesic and G. Q. Lu, *Journal of Catalysis*, 2008, **258**, 366-377.
57. M. Breysse, J. L. Portefaix and M. Vrinat, *Catalysis Today*, 1991, **10**, 489-505.
58. K. D. Bronsema, J. L. De Boer and F. Jellinek, *Zeitschrift für anorganische und allgemeine Chemie*, 1986, **540**, 15-17.
59. I. T. Ghampson, C. Sepúlveda, R. Garcia, L. R. Radovic, J. L. G. Fierro, W. J. DeSisto and N. Escalona, *Applied Catalysis A: General*, 2012, **439–440**, 111-124.
60. V. N. Bui, D. Laurenti, P. Afanasiev and C. Geantet, *Applied Catalysis B: Environmental*, 2011, **101**, 239-245.
61. M. Ferrari, B. Delmon and P. Grange, *Carbon*, 2002, **40**, 497-511.
62. C. Sepúlveda, N. Escalona, R. García, D. Laurenti and M. Vrinat, *Catalysis Today*, 2012, **195**, 101-105.
63. E. O. Odebunmi and D. F. Ollis, *Journal of Catalysis*, 1983, **80**, 56-64.
64. C. Zhao, Y. Kou, A. A. Lemonidou, X. Li and J. A. Lercher, *Angewandte Chemie International Edition*, 2009, **48**, 3987-3990.
65. V. N. Bui, G. Toussaint, D. Laurenti, C. Mirodatos and C. Geantet, *Catalysis Today*, 2009, **143**, 172-178.
66. D. A. Netzel, F. P. Miknis, J. M. Mitzel, T. Zhang, P. D. Jacobs and H. W. Haynes Jr, *Fuel*, 1996, **75**, 1397-1405.
67. T. R. Viljava, R. S. Komulainen and A. O. I. Krause, *Catalysis Today*, 2000, **60**, 83-92.
68. J. A. Moulijn, A. E. van Diepen and F. Kapteijn, *Applied Catalysis A: General*, 2001, **212**, 3-16.
69. C. Leyva, M. S. Rana, F. Trejo and J. Ancheyta, *Catalysis Today*, 2009, **141**, 168-175.
70. A. Gupta, G. Chen, P. Joshi, S. Tadigadapa and Eklund, *Nano Letters*, 2006, **6**, 2667-2673.
71. A. C. Ferrari, J. C. Meyer, V. Scardaci, C. Casiraghi, M. Lazzeri, F. Mauri, S. Piscanec, D. Jiang, K. S. Novoselov, S. Roth and A. K. Geim, *Physical Review Letters*, 2006, **97**, 187401.
72. C. Lee, H. Yan, L. E. Brus, T. F. Heinz, J. Hone and S. Ryu, *ACS Nano*, 2010, **4**, 2695-2700.
73. J. D. Benck, Z. Chen, L. Y. Kuritzky, A. J. Forman and T. F. Jaramillo, *ACS Catalysis*, 2012, **2**, 1916-1923.
74. E. Furimsky, J. A. Mikhlin, D. Q. Jones, T. Adley and H. Baikowitz, *The Canadian Journal of Chemical Engineering*, 1986, **64**, 982-985.